Multiferroic phase transitions in manganites $R\mathrm{MnO_3}$: A two-orbital double exchange simulation*

Tao Yong-Mei(陶永梅)[a)b)], Lin Lin(林 林)[a)], Dong Shuai(董 帅)[a)], and Liu Jun-Ming(刘俊明)[a)†]

[a)] *Laboratory of Solid State Microstructures, Nanjing University, Nanjing* 210093, *China*

[b)] *Jiangsu Laboratory of Advanced Functional Materials, Changshu Institute of Technology, Changshu* 215500, *China*

(Received 16 February 2012; revised manuscript received 24 February 2012)

The semi-quantum two-orbital exchange model is used to investigate the effect of small rare-earth ion substitution on orthorhombic $R\mathrm{MnO_3}$ with A-type antiferromagnetic order, using the Monte Carlo algorithm, exact diagonalization, and zero-temperature optimization approaches. It is revealed that the substitution results in a rich multiferroic phase diagram where the coexisting A-type antiferromagnetic phase and spiral spin phase, pure spiral spin phase, coexisting spiral spin phase, the E-type antiferromagnetic phase, and the pure E-type antiferromagnetic phase emerge in sequence. The multiferroic phase transitions modulate substantially the electric polarization, which is consistent qualitatively with recent experiments.

Keywords: multiferroic phase, R-site doping, two-orbital exchange model

PACS: 75.47.Lx, 64.75.Gh, 75.30.Kz, 64.70.Rh **DOI:** 10.1088/1674-1056/21/10/107502

1. Introduction

The coexistence of frustrated spin order and ferroelectric (FE) polarization (P) is commonly referred to as multiferroic behaviour.[1−3] Due to the intercoupling between the spin order and electric order which allows the electric control of spin moment and the magnetic control of polarization P, multiferroics have attracted attention and promise a number of technological applications.[4−10] The ABO_3-type perovskite manganites ($R\mathrm{MnO_3}$, R represents a rare earth species) each with an orthorhombic structure, have been the most often visited classes of multiferroic compounds, especially since the discovery of ferroelectricity in systems of spiral (cycloidal) spin order.[11−13] For $R\mathrm{MnO_3}$, the magnetic ground state is intrinsically related to the R-site ionic radius which controls the distortion of the $\mathrm{MnO_6}$ octahedron. When the R-site is occupied by a large species, e.g. La, Pr, Nd, and Sm, the A-type antiferromagnetic (AFM) order (A-phase) is preferred. It will be replaced by the spiral spin ordered phase (S-phase) when the R-site is occupied with Tb and Dy. If even smaller ions (Ho to Lu) take the R-site, the ground state comes to the E-type AFM order (E-phase) on the assumption that it has an orthorhombic symmetry rather than a hexagonal structure.[11,14−18] A sketch of the magnetic phase diagram for $R\mathrm{MnO_3}$ is shown in Fig. 1(a) for reference.

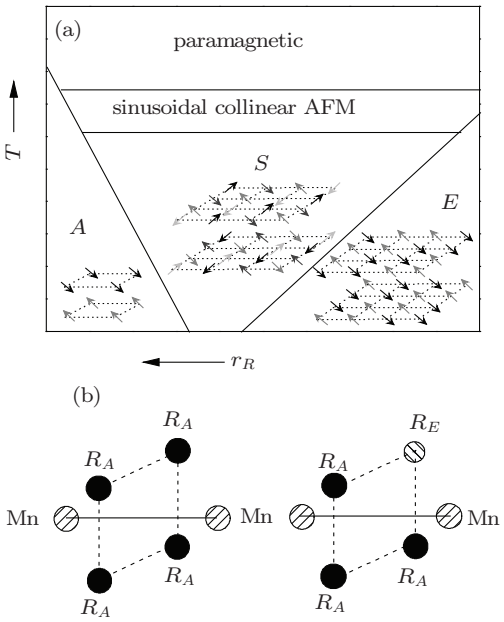


Fig. 1. (a) A sketch of the magnetic phase diagram for orthorhombic $R\mathrm{MnO_3}$ manganites, where r_R is the R-site ionic size, symbols A, S, and E, denote the A-phase, S-phase, and E-phase respectively. (b) The $R\mathrm{MnO_3}$ ionic configuration without oxygen ions.

*Project supported by the National Natural Science Foundation of China (Grant Nos. 51031004, 11004027, and 11074113), the National Basic Research Program of China (Grant Nos. 2011CB922101 and 2009CB929501), and the Priority Academic Program Development of Jiangsu Provincial Higher Education Institutions, China.

†Corresponding author. E-mail: liujm@nju.edu.cn

© 2012 Chinese Physical Society and IOP Publishing Ltd

Recent experiments revealed that those manganites with either an S-phase or an E-phase exhibit nonzero P below the specific spin ordering temperature (T), and polarization P is induced by the specific spin order. For the S-phase, the underlying mechanism is conceptually described by the asymmetrical exchange model based on the inverse Dzyaloshinskii–Moriya (DM) interaction,[19,20] while that for the E-phase can be explained by the symmetric exchange striction mechanism.[21,22] Nevertheless, a substantial challenge to these multiferroics is the low Curie point ($T_{\rm FE}$) and small P, while no sufficient magnetization is available due to their AFM nature. An alternative method to improve these properties is appealing.

First, it is desirable to extend the S-phase region into the A-phase region via proper modulation of the R-site ionic radius by such a substitution that additional multiferroics can be synthesized. Typical examples to illustrate this approach include $Sm_{1-x}Y_xMnO_3$ ($x = 0.4 \sim 0.5$) and $Eu_{1-x}Y_xMnO_3$ ($0.3 \leq x \leq 0.5$).[23–26] Second, it is noted that the S-phase is more favourable than the E-phase because of magnetoelectric (ME) control.[18] Thus, it is predicted that a RMnO$_3$ with an E-phase offers a polarization much larger than that generated from a S-phase.[18,22] This immediately allows a suggestion that a system with a S-phase plus an E-phase may offer both a large P and a remarkable ME response.[18,27] For $Eu_{0.1}Y_{0.9}MnO_3$, a fairly large $P \sim 800$ μC/m^2 and remarkable response of P to the external magnetic field h were revealed,[18] which we argue here arises from the S-phase and E-phase coexistence. Nevertheless, a comprehensive theory on the spin ordered phase transitions appears to not yet be available, which is, however, of special significance.

In this work, we focus on the semi-quantum two-orbital double exchange (TO-DE) model, which is specifically suited to manganites, in order to capture the physics for the spin ordered phase transitions across the A-phase, S-phase, and E-phase by a substitution approach,[15] and thus to understand the multiferroic behaviours. We address three issues: (i) whether it is accessible to obtain the S-phase in the A-phase; (ii) whether the S-phase and E-phase co-exist in a well-controlled manner; (iii) how the P in such a state of coexistence is modulated. While the classical Mochizuki–Furukawa model was used to investigate these issues,[16,17] the present quantum model may have a comprehensive insight into the physics of multiferroic phase transitions, including the electronic structure.

2. Model and methods

For simplification, we start from the TO-DE model in a two-dimensional (2D) $L\times L$ (12×12) square lattice on the x–y plane under the periodic boundary conditions, which represent the Mn ionic plane of RMnO$_3$ in an orthorhombic structure. The Hamiltonian for the TO-DE model is given by[15,28]

$$\begin{aligned} H = & -\sum_{\langle ij\rangle,\alpha\beta} t^r_{\alpha\beta}\Omega_{ij}c^\dagger_{i\alpha}c_{j\beta} + \sum_{\langle ij\rangle} J^{\rm AF}_{ij}\boldsymbol{S}_i\cdot\boldsymbol{S}_j \\ & + \sum_{[ij]} J^{2b}_{ij}\boldsymbol{S}_i\cdot\boldsymbol{S}_j + \lambda\sum_i (Q_{2i}\tau_{xi} + Q_{3i}\tau_{zi}) \\ & + \frac{1}{2}\sum_i (Q^2_{2i} + Q^2_{3i}), \end{aligned} \tag{1}$$

where the first term on the right-hand side of the above expression is the DE kinetic energy of an e_g electron, $\alpha = |x^2 - y^2\rangle$ and $\beta = |3z^2 - r^2\rangle$ are the two Mn-e_g orbitals; $c^\dagger_{i\alpha\sigma}(c_{j\beta\sigma})$ is the creation (annihilation) operator for the e_g electron carrying spin σ on site i; $\Omega_{ij} = \cos(\theta_i/2)\cos(\theta_j/2) + \sin(\theta_i/2)\sin(\theta_j/2)\exp[-{\rm i}(\Phi_i - \Phi_j)]$ with θ_i and Φ_i being the angles of the t_{2g} spin S_i in the spherical coordinates. If the actual hopping amplitudes $t^r_{\alpha\beta}$ are taken into account the different overlaps between the orbits along the x axis and y axis of the lattice are: $t^x_{\alpha\alpha} = t^y_{\alpha\alpha} = 3t^x_{\beta\beta} = 3t^y_{\beta\beta} = 3t_0/4$, $t^y_{\alpha\beta} = t^y_{\beta\alpha} = -t^x_{\alpha\beta} = -t^x_{\beta\alpha} = \sqrt{3}t_0/4$, and t_0 (~ 0.2 eV–0.5 eV) is chosen as the energy unit. The second and third terms on the right-hand side in Eq. (1) are the superexchange interactions between the NN and NNN t_{2g} spins along the b axis. We choose ($J^A_{\rm AF}$, $J^A_{\rm 2b}$)=(0.08, 0.005) and ($J^E_{\rm AF}$, $J^E_{\rm 2b}$)=(0.097, 0.011), where the superscripts A and E refer to the A-phase and E-phase, respectively. Intentionally, for a lattice randomly doped with smaller ions at the R-site, one considers the R–O layer neighbouring to the MnO_2 plane as shown in Fig. 1(b). It is easy to obtain $J^{\rm AF}_{ij} = (nn^A_{ij}J^A_{\rm AF} + nn^E_{ij}J^E_{\rm AF})/4$ and $J^{\rm 2b}_{ij} = (nnn^A_{ij}J^A_{\rm 2b} + nnn^E_{ij}J^E_{\rm 2b})/2$, which are determined mainly by the four NN and two NNN R-site cations respevtively,[27] where nn and nnn denote the numbers of NN and NNN R-site cations. The substitution level is thus defined as $x = \sum_{ij} nn^E_{ij}/4L^2$. The fourth term on the right-hand side in Eq. (1) is the electron–phonon coupling arising from the interaction between the e_g electron and the MnO_6 octahedra distortion, and λ is the coupling constant with Q_{2i} and Q_{3i} scaling the (x^2–y^2) and ($3z^2$–r^2)-type Jahn–Teller distortions, respectively. We choose

$\lambda|Q_{2i}| = 1.5$ and $Q_{3i} = -|Q_{2i}|/\sqrt{3}$ without losing the generality.[15] The orbital pseudospin operators are $\tau_{xi} = \sum_\sigma (c^\dagger_{\mathrm{i}\alpha\sigma} c_{\mathrm{i}\beta\sigma} + c^\dagger_{\mathrm{i}\beta\sigma} c_{\mathrm{i}\alpha\sigma})$ and $\tau_{zi} = \sum_\sigma (c^\dagger_{\mathrm{i}\alpha\sigma} c_{\mathrm{i}\alpha\sigma} - c^\dagger_{\mathrm{i}\beta\sigma} c_{\mathrm{i}\beta\sigma})$. The last term on the right-hand side of Eq. (1) is the elastic energy of the phonons. Typically, the temperature chosen for running the simulation is $T = 0.002$ for the ground state.

In order to identify the spin phase, we evaluate spin configuration in real space and calculate the spin structure factor $C(\boldsymbol{k}) = \sum_{ij} (\boldsymbol{S}_i \cdot \boldsymbol{S}_j) \exp[\mathrm{i}\boldsymbol{k} \cdot (\boldsymbol{r}_i - \boldsymbol{r}_j)]/L^4$ in the momentum space. the inverse DM mechanism and the symmetric exchange striction (double-exchange) mechanism contribute to the polarization P, i.e. it is generated by the S-phase and E-phase, respectively. They can be expressed as

$$P^{\mathrm{DM}} \propto \frac{1}{L^2} \left\langle \sum_{\langle ij \rangle} |\boldsymbol{e}_{ij} \times (\boldsymbol{S}_i \times \boldsymbol{S}_j)| \right\rangle_{\mathrm{T}},$$
$$P^{\mathrm{DE}} \propto \frac{1}{L^2} \left\langle \sum_{\langle ij \rangle} r_{ij} \sqrt{1 + \boldsymbol{S}_i \cdot \boldsymbol{S}_j} \right\rangle_{\mathrm{T}}, \qquad (2)$$

where $\boldsymbol{e}_{ij}$ denotes the unit vector connecting sites i and j,[19,20] and r_{ij} denotes the oxygen displacement between the i-th and j-th Mn ions, and the $\langle \cdots \rangle_{\mathrm{T}}$ represents the averaging of thermal configuration. Ideally, P^{DM} is dominant in the S-phase and related to the spin–orbit coupling, while in the E-phase the Mn ion displacements are staggered in the $+-+-$ pattern along the x axis and y axis and P^{DE} is independent of the spin–orbit coupling.[21,22]

The Monte Carlo (MC) procedure of the $\mathrm{t_{2g}}$ spin is employed for the present calculation. At each MC step, the fermionic sector of the Hamiltonian is exactly diagonalized.[15,27] The initial 15000 MC steps are discarded for equilibration and the subsequent 5000 MC steps are retained for data collection. Finally, the data are submitted to the zero-T optimization to confirm the ground state.

3. Results and discussion

Prior to considering the mixture of the A-phase and the E-phase, we first look at the pure A-phase and E-phase. At x=0, the ground state is in the A-phase where all the in-plane spins align in the ferromagnetic order. For $x = 1.0$, a pure E-phase is obtained with an up-up-down-down spin order along the x axis or the y axis, and it consists of ferromagnetic zigzag chains where the two neighbouring chains are antiparallel to the spin alignment.[15] Then we focus on the smaller ion substitution at the R-site for the A-phase, which leads to more than the simple coexistence of the A-phase and E-phase but a sequence of spin ordered phase transitions. Several pictures of the spin configurations for various x ($x = 0.1$, 0.5, 0.6, and 0.7) are shown in Fig. 2. It is identified that the spin order is sensitive to the substitution. A low level ($x = 0.1$) is sufficient to partially destroy the A-phase (Fig. 2(a)). Instead of the expected appearance of the local E-phase due to the substitution, we observe the local S-phase in coexistence with the A-phase. This surprising outcome indicates that the S-phase, which is an ingredient for P generation, can be induced by the substitution with small R ions. Furthermore, the phase coexistence is indeed possible by means of such a substitution, while it is challenging to its detection experimentally.

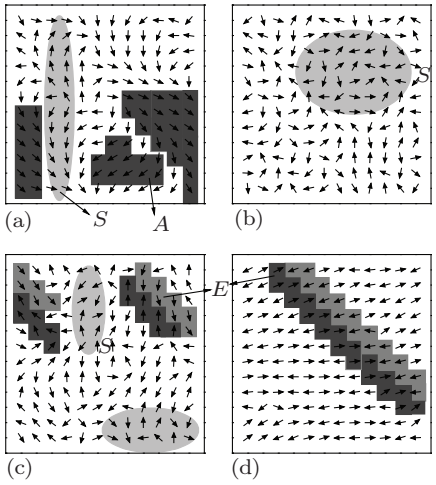


Fig. 2. Mn spin structures for (a) $x = 0.1$ with a coexisting A-phase and S-phase, (b) $x = 0.5$ with a pure S-phase, (c) $x = 0.6$ with a coexisting S-phase and E-phase, and (d) $x = 0.7$ with a pure E-phase.

With x increasing, the S-phase increases in its volume fraction in parallel with a suppressed A-phase until $x \sim 0.35$, beyond which the whole lattice is occupied with the S-phase evidenced with one example shown in Fig. 2(b) at $x = 0.50$. The value of x further increasing up to 0.6 leads to the appearance of the E-phase as shown in Fig. 2(c) for $x = 0.6$, and the whole lattice is filled with the E-phase at $x \geq 0.7$ as shown in Fig. 2(d). Therefore, one understands that R-site substitution with a smaller species can lead to a sequence of the A-phase plus the S-phase, pure S-phase, S-phase plus E-phase, and pure E-phase.

To further confirm these phase transitions, a spin structure factor $C(\boldsymbol{k})$ is evaluated and shown in Fig. 3.

At $x = 0.1$, a peak of $C(\boldsymbol{k})$ appears at $\boldsymbol{k} = (0, 0)$, indicating an in-plane FM order. The other two main peaks at $\boldsymbol{k} = \pm\pi(1, 1)/12$ correspond to the S-phase with a spiral periodicity of 12 along the x axis and y axis respectively, confirming the coexistence of the A-phase and the S-phase. At $x = 0.5$, the peak at $\boldsymbol{k} = (0, 0)$ disappears completely, indicating that no more A-phase appears, while only two peaks at $\boldsymbol{k} = \pm\pi(1, 1)/6$ for the S-phase are available. For $x = 0.6$, there are at least ten visible peaks appearing respectively at $\boldsymbol{k} = \pm\pi(3, 2)/12$, $\pm\pi(2, 3)/12$, $\pm\pi(1, 1)/6$, $\pm\pi(1, 3)/12$, and $\pm\pi(1, 1)/4$. The first eight peaks refer to the S-phase and the last two peaks feature the E-phase. Figure 3(d) shows the $C(\boldsymbol{k})$ for the pure E-phase with two peaks at $\boldsymbol{k} = \pm\pi(1, 1)/4$.

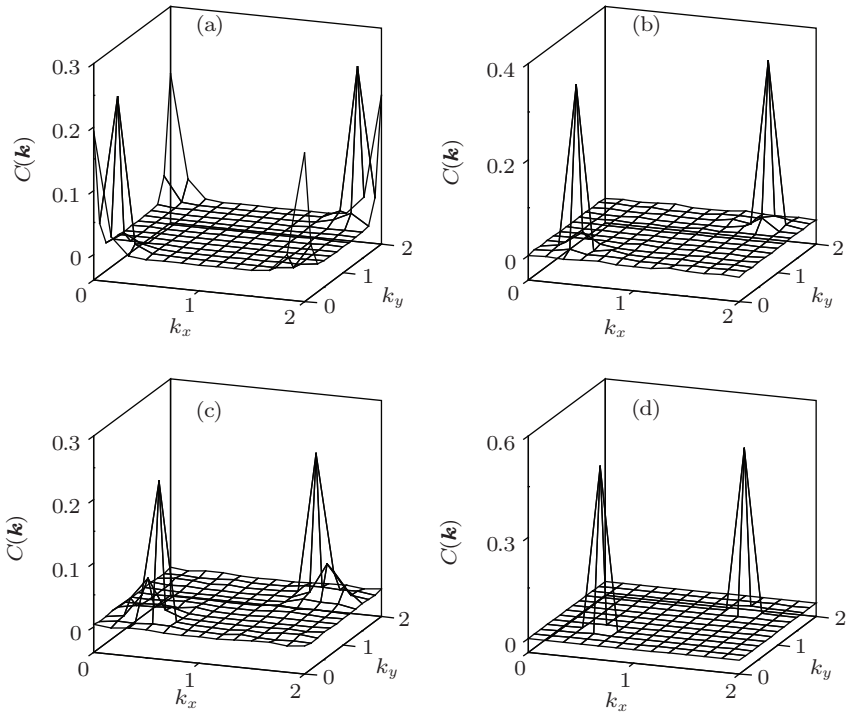


Fig. 3. Calculated $C(\boldsymbol{k})$ spectra for (a) $x = 0.1$, (b) $x = 0.5$, (c) $x = 0.6$, and (d) $x = 0.7$, respectively.

To achieve the ferroelectricity, it is necessary to check the electronic structure in response to the substitution. The calculated densities of states (DOSs) for all these samples and evaluated band gap Δ are presented in Fig. 4. While the DOS spectra shows not much difference for these substitution levels, the band gap Δ is irrelevant to x until $x \sim 0.55$ ($\Delta \sim 1.75t_0 = 0.35$ eV–0.875 eV), beyond which Δ is observed to rapidly increase up to $\Delta \sim 1.82t_0 = 0.364$ eV–0.91 eV for the E-phase ($x = 1.0$). No anomaly is identified for the phase coexistence regime. The $\Delta \sim x$ dependence is quite reasonable for manganite, and one sees that the A-phase in the 2D lattice is in-plane FM-ordered while the E-phase prefers to align in the direction anti-parallel to the diagonal direction. Referring to the TO-DE model, the AFM order obviously has the biggest gap with respect to the in-plane FM order, which is consistent with the present simulation result. The S-phase can be viewed as a superposition of the FM alignment and AFM alignment.

The evaluated polarization components, P^{DM} and P^{DE}, each as a function of x are presented in Fig. 5(a), in which it is noted that they are not comparable in value. Due to the limit lattice size, the simulation data are scattered and thus the configuration averaging is performed over quite a big number of samples. The dependences of P^{DM} and P^{DE} on x are evident. It is noted that the A-phase has no P ($P^{\mathrm{DM}} < 0.06$ and $P^{\mathrm{DE}} = 0$), while the S-phase contributes to P^{DM}, explaining the rapid increase of P^{DM} with x increasing until $x \sim 0.35$. Afterwards, P^{DM} begins to fall down, accompanied with the appearance of non-zero P^{DE} since the E-phase grows from the S-phase at $x \geq 0.6$. P^{DE} increases steeply with x increasing and becomes saturated at $x \geq 0.7$.

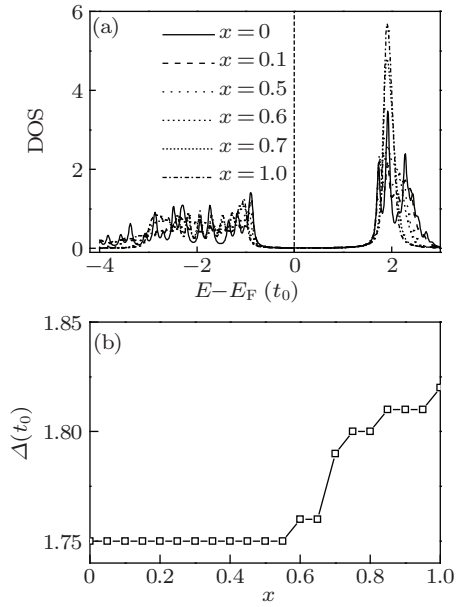


Fig. 4. (a) Calculated DOSs for $x = 0$, 0.1, 0.5, 0.6, 0.7, and 1.0, respectively, and (b) evaluated energy gap $\Delta(x)$.

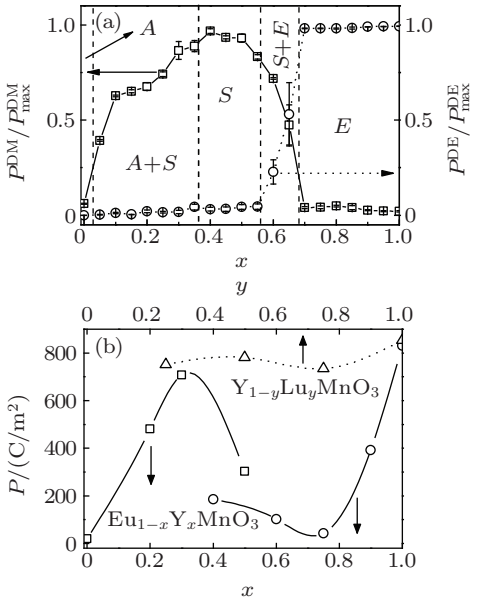


Fig. 5. (a) Evaluated multiferroic phase diagrams and polarization components, P^{DM} and P^{DE} (normalized by their maximal values respectively), each as a function of x. Here symbols A, S, and E denote the A-phase, S-phase, and E-phase respectively. (b) Measured polarization data on $Eu_{1-x}Y_xMnO_3$ cited from Ref. [25] (square dots) and Ref. [18] (circle dots), and measured data on $Y_{1-y}Lu_yMnO_3$ cited from Ref. [18] (up-triangle dots). It is noted that a one-to-one quantitative correspondence between x and y/z makes no sense and only a qualitative comparison is shown here.

To sum up the simulated results, one may propose a low-T multiferroic phase diagram as plotted in Fig. 5(a). This phase diagram illustrates clearly the transitions of the magnetic ground state from the A-phase to the A-phase plus S-phase to the S-phase to the S-phase plus E-phase to the E-phase, in sequence, with the substitution level (x) increasing. This consequence is easy to understand if one considers the NN and NNN interactions in the substituted lattice. In our model, the substitution is done by replacing the smaller J^{AF} and J^{2b} values which favour the A-phase with larger J^{AF} and J^{2b} values which favour the E-phase. This treatment corresponds to a realistic case, taking $Sm_{1-x}Y_xMnO_3$ for example, where a substitution of larger Sm^{3+} with smaller Y^{3+} leads to a more serious local MnO_6 octahedron distortion in $RMnO_3$ manganite, characterized by a gradual decrease of the Mn–O–Mn bond angle away from 180°. It is noted that the E-phase always has smaller Mn–O–Mn bond angle than the A-phase.

Finally, we compare qualitatively our simulated results with recent experimental data, while it should be noted that no complete set of data covering the whole composition range for one system is available. In Fig. 5(b) the polarization component data for $Eu_{1-y}Y_yMnO_3$ and $Y_{1-z}Lu_zMnO_3$ versus the substitution level x,[18,25] are plotted, in which it is noted that the substitution levels y and z are not in one-to-one correspondence with x in our simulation (Fig. 5(a)). For $Eu_{1-y}Y_yMnO_3$ where $EuMnO_3$ favours the A-phase and $YMnO_3$ favours the E-phase, a low y ($y \leq 0.3$) results in the S-phase, accompanied with polarization P ensuing and increasing rapidly with y.[25] A coexisting A-phase plus S-phase between the pure A-phase and pure S-phase was confirmed for $Nd_{1-y}Y_yMnO_3$ ($0.4 \leq y \leq 0.55$) by neutron powder-diffraction.[29] For $Sm_{0.6}Y_{0.4}MnO_3$, $Sm_{0.5}Y_{0.5}MnO_3$, and $Eu_{1-y}Y_yMnO_3$ ($0.3 \leq y \leq 0.5$), the substitution covers the intermediate range, the measured polarization can be nearly completely suppressed by a magnetic field of several Tesla, indicating the pure S-phase in these materials.[23–25] These results are roughly consistent with the simulated $P^{DM}(x)$. Nevertheless, at high y ($y \sim 0.9$) for $Eu_{1-y}Y_yMnO_3$, the measured P increases with y increasing and particularly it cannot be completely suppressed with a finite magnetic field,[18] suggesting the coexistence of the S-phase and the E-phase, while it is known that the E-phase is robust against a magnetic field unless the field is very high. This behaviour fits qualitatively to $P^{DE}(x)$. For the pure E-phase state, the simulated $P^{DE}(x)$ remains roughly unchanged against x. Indeed, the data on $Y_{1-z}Lu_zMnO_3$ show nearly no z-dependence of the measured P, which is consistent with the simulated $P^{DE}(x)$ at a high value of x.[18]

Certainly, the above comparison is qualitative and these multiferroic phase transitions need additional

checks. In addition, the over-simplified treatments in our simulations should be mentioned. First, the third NN interactions, smaller than the NN and NNN interactions, are neglected. Second, for computability considerations, the effect from the magnetic R-site ions is excluded. The 2D model cannot distinguish the ab-cycloidal order from the bc-cycloidal order which is available in multiferroic manganites. However, the main conclusion here remains unchanged in the sense that the major physical ingredient is captured.

4. Conclusions

In the present paper, the multiferroic phase transitions in orthorhombic $R\mathrm{MnO_3}$ associated with the substitution of small rare-earth ion into the A-phase are investigated in the framework of a semi-quantum TO-DE model. The substitution leads to successive transitions of the spin order from the A-phase to the coexisting A-phase and S-phase to the pure S-phase to the coexisting S-phase and E-phase to the pure E-phase, accompanied with corresponding modulation of the electric polarization. Our simulations explain qualitatively recent experiments on various multiferroic manganites.

References

[1] Cheong S W and Mostovoy M 2007 *Nature Mater.* **6** 13

[2] Wang K F, Liu J M and Ren Z F 2009 *Adv. Phys.* **58** 321

[3] Tokura Y and Seki S 2010 *Adv. Mater.* **22** 1554

[4] Scott J F 2007 *Nature Mater.* **6** 256

[5] Spaldin N A and Fiebig M 2005 *Science* **309** 391

[6] Zhang Y, Deng C Y, Ma J, Lin Y H and Nan C W 2008 *Chin. Phys.* B **17** 3910

[7] Ge B H, Li F H, Li X M, Wang Y M, Chi Z H and Jin C Q 2008 *Chin. Phys.* B **17** 3163

[8] Dong S and Liu J M 2010 *Prog. Phys.* **30** 1 (in Chinese)

[9] Dong S and Liu J M 2012 *Mod. Phys. Lett.* B **26** 1230004

[10] Zhong C G, Jiang Q, Huai F J and Wang G C 2009 *Acta Phys. Sin.* **58** 3491 (in Chinese)

[11] Goto T, Kimura T, Lawes G, Ramirez A P and Tokura Y 2004 *Phys. Rev. Lett.* **92** 257201

[12] Kimura T, Goto T, Shintani H, Ishizaka K, Arima T and Tokura Y 2003 *Nature* **426** 55

[13] Yamasaki Y, Sagayama H, Abe N, Arima T, Sasai K, Matsuura M, Hirota K, Okuyama D, Noda Y and Tokura Y 2008 *Phys. Rev. Lett.* **101** 097204

[14] Kimura T, Lawes G, Goto T, Tokura Y and Ramirez A P 2005 *Phys. Rev.* B **71** 224425

[15] Dong S, Yu R, Yunoki S, Liu J M and Dagotto E 2008 *Phys. Rev.* B **78** 155121

[16] Mochizuki M and Furukawa N 2009 *Phys. Rev.* B **80** 134416

[17] Mochizuki M, Furukawa N and Nagaosa N 2011 *Phys. Rev.* B **84** 144409

[18] Ishiwata S, Kaneko Y, Tokunaga Y, Taguchi Y, Arima T and Tokura Y 2010 *Phys. Rev.* B **81** 100411

[19] Mostovoy M 2006 *Phys. Rev. Lett.* **96** 067601

[20] Moriya T 1960 *Phys. Rev.* **120** 91

[21] Picozzi S, Yamauchi K, Sanyal B, Sergienko I A and Dagotto E 2007 *Phys. Rev. Lett.* **99** 227201

[22] Sergienko I A, Sen C and Dagotto E 2006 *Phys. Rev. Lett.* **97** 227204

[23] O'Flynn D, Tomy C V, Lees M R, Daoud-Aladine A and Balakrishnan G 2011 *Phys. Rev.* B **83** 174426

[24] Yamasaki Y, Miyasaka S, Goto T, Sagayama H, Arima T and Tokura Y 2007 *Phys. Rev.* B **76** 184418

[25] Hemberger J, Schrettle F, Pimenov A, Lunkenheimer P, Ivanov V Yu, Mukhin A A, Balbashov A M and A Loidl 2007 *Phys. Rev.* B **75** 035118

[26] Okuyama D, Ishiwata S, Takahashi Y, Yamauchi K, Picozzi S, Sugimoto K, Sakai H, Takata M, Shimano R, Taguchi Y, Arima T and Tokura Y 2011 *Phys. Rev.* B **84** 054440

[27] Lu C L, Dong S, Wang K F and Liu J M 2010 *Appl. Phys.* A **99** 323

[28] Hotta T, Feiguin A and Dagotto E 2001 *Phys. Rev. Lett.* **86** 4922

[29] Landsgesell S, Maljuk A, Hansen T C, Prokhnenko O, Aliouane N and Argyriou D N 2009 *Phys. Rev.* B **80** 014412